SIMULTANEOUS POSITION AND STIFFNESS DISTRIBUTION CONTROL OF ELASTIC REDUNDANT CLOSED-LOOP MECHANISM

DAISUKE MATSUURA, NOBUYUKI IWATSUKI, MASAFUMI OKADA

Abstract. The present paper discusses a new design of robotic manipulator having redundant closed-loop mechanism with elastic passive joints. The proposed design is aiming to be utilized for developing robots that are capable to work in complicated and unpredictable environments such as natural environments, disaster sites or daily human living space. In order to deal with various contact conditions between surrounding objects and robot, effective approach called flexibility control is figured out. This methodology includes planning and optimization of force application not only on single considered point on an object but also its distribution among certain contact area. This paper defines the ability to optimize stiffness distribution at a number of contact points as "flexibility" and proposes elastic closed-loop mechanism which has a serial chain of revolute joints with torsion coil springs anchored at two ends to form a closed-loop, as a lightweight and supple hyper redundant mechanism. Output stiffness is formulated based on the minimization of potential energy, the balancing of internal force and the velocity constraint to construct a closed-loop mechanism. Joint input to obtain both the desired stiffness distribution and desired output position simultaneously is derived from partial derivative of the output stiffness and compensation by a learning control scheme. Motion control experiments with a 10R elastic closed-loop robot demonstrate the effectiveness of the proposed control scheme.

Key words: elastic closed-loop mechanism, flexibility control, position and stiffness distribution control.

1. INTRODUCTION

Hyper redundant mechanism having extremely huge degrees of freedom against the dimension of workspace is useful to develop dexterous robotic systems working in complicated and unpredictable environments such as natural environment, disaster sites or daily human living space due to the capability of adapting to unpredictable environment while achieving many objectives. During the actual operation of this kind of robots, contact between surrounding objects and

Tokyo Institute of Technology, Department of Mechanical Sciences and Engineering, Graduate School of Science and Engineering, 2-12-1 Ookayama Meguro-ku, Tokyo 152-8552, Japan. E-mail: matsuura@mech.titech.ac.jp, Tel, Fax: +81-3-5734-2177

Rom. J. Techn. Sci. – Appl. Mechanics, Vol. 58, N^{os} 1–2, P. 107–126, Bucharest, 2013

robot will be frequently occurs under both controlled and uncontrolled situations, such as manipulation, carrying specific object or unpredictable collision with obstacle. In order to deal with such various situations, robot should optimize not only positions and velocities of certain output links but also force distribution among whole contact area. In addition, links to contact with objects should be selected among a number of candidates according to the current contact condition, instead of using preliminary defined output points, so that capability of adaptation of the robot can be maximized.

In previous researches aiming to control output force of redundant robots, a number of methods based on force control [1–4], compliance control [5–7] or impedance control [8–11] have been proposed. However, those conventional methods considered only specific output links to give desired command values to be achieved, and assumed degrees of freedom was not so many. Thus they were not quite adaptive on contact condition control. In addition, implementing all active joints by conventional electric motors is not practical because due to the increasing of mass and inevitable time delay of electric control, such robot's motion will be slowed down and capability to react to impaction force due to sudden contact like collision will be lost. In order to solve this problem, a part of joint should be composed by passive elastic elements to guarantee both large degrees of freedom and lightweight mechanism, while achieving large workspace. From this point of view, many approaches such as utilizing nonlinear profile of mechanical stiffness due to the change of kinematic configuration [12–14] or dexterous manipulation considering elastic deformation of soft fingertip [15–18] have been attempted. However, these methods did not consider controlling output stiffness distribution at multiple contact points, and that was also difficult to achieve wide range of stiffness change and large workspace purely relying on the elastic deformation of conventional springs.

The authors have been working on design and motion control of hyper redundant mechanism such as learning control based on linear combination of error history [19] and optimization of multiple objective functions to maximize both the assistability of current task and capability to achieve future task [20]. In this paper, an effective solution for simultaneous control of motion and output force distribution control by utilizing the capability of redundant mechanism on widely changing kinematic configuration will be proposed. When a redundant robot has kinematic chains composed of elastic joints forming a closed-loop mechanism, output links to contact with external objects can be chosen among that part and distribution of output force can be controlled based on the internal force balance. Namely, redundant closed-loop mechanism having elastic joint is an effective solution to perform the above mentioned force distribution control. Based on this principle, "Flexibility Control" concept [21] which represents an ability of hyper redundant robot to achieve a desired force distribution on arbitrary target objects while holding target output position is figured out. An elastic redundant closed-loop mechanism having a serial chain of elastic joints that have torsion coil springs on their revolute joints is designed to establish the flexibility control concept. In the formulation of the flexibility control scheme, the output stiffness which describes the relationship between external loads exerted on each link and resulting change of mechanical configuration is formulated as the first step. Then the partial derivative of the output stiffness is employed to obtain the optimum joint input, together with the learning control based on linear combination of error history [19] to achieve both the desired output stiffness distribution and output position at the same time. The established control scheme is applied to motion control experiment of a 10R planar elastic closed-loop robot manipulator.

2. MECHANISM DESIGN AND TASK DEFINITION

Let us consider an elastic closed-loop mechanism shown in Fig. 1. On the left and right bottom of the figure, the mechanism has two serial chains of active joints called “Actuator Part”, having N_ℓ and N_r of revolute joints, $J_{\mathrm{L}1}$, ... , $J_{\mathrm{L}N\ell}$ and $J_{\mathrm{R}1}$, ... , $J_{\mathrm{R}N\mathrm{r}}$, and connected to the ground at two ends, $J_{\mathrm{L}1}$ and $J_{\mathrm{R}1}$, respectively. In between the two actuator parts, a serial chain of elastic joints called “Spring Part” having N_e of revolute joints, J_1 , ... , $J_{N\mathrm{e}}$, is connected, and each elastic joint has a torsion coil spring on its rotation axis. Arbitrary links of the spring part can be used as end effectors to contact with external objects, and control points are located on the center of all those links in order to control output stiffness distribution. In addition, one of the control points is chosen as an output point for position control. This position control is performed as a main task which should be achieved precisely. The output stiffness distribution control is achieved as a sub task which should be achieved as much as possible, next to the main task. The characteristic of this mechanism is that distribution of output stiffness on spring part can be calculated only by considering the configuration of the spring part when the joint stiffness of actuator part is assumed to be infinite. Although position and orientation of the tip links of both actuated parts affect to them, this effect becomes relatively small when the number of joint in spring part is larger than that in actuator part. Because of this principle, stiffness analysis is performed very easily, and stiffness distribution control can be done only by taking care of the distance between two ends of spring part and inclination angle of the line connecting those two joints. In addition, the mechanism is capable of changing its configuration widely than conventional parallel mechanism due to less mechanical constraints, and thus can have large workspace.

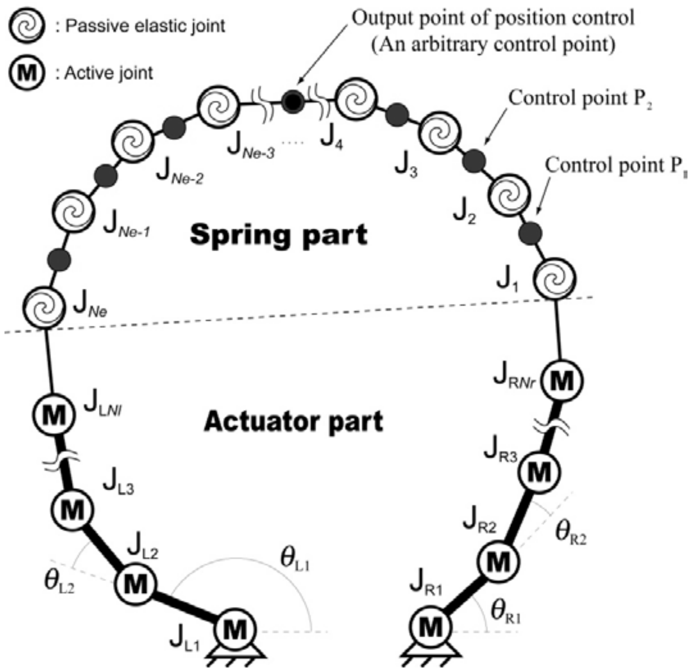

Fig. 1 – Elastic redundant closed-loop mechanism.

Let M and α represent the degrees of freedom of workspace and the constraint condition to construct a closed-loop mechanism respectively, the redundant degrees of freedom that can be used for stiffness distribution control is

$$M_{\mathrm{s}} = N_{\mathrm{I}} + N_{\mathrm{r}} - M - \alpha . \tag{1}$$

Fig. 2 shows the process flow of the flexibility control scheme to achieve both commanded position and stiffness distribution. Firstly, command position of the main task and stiffness distribution of the subtask are given, and initial configuration of the actuator part is determined (Fig. 2-(1)). Subsequently, configuration of the spring part is obtained based on minimization of the summation of kinematic energy stored in all torsional springs. Location of the output point for the position control is also obtained at this moment (Fig. 2-(2)). In the third step, output stiffness distribution on the spring part is calculated under the consideration of the balance of internal force (Fig. 2-(3)). From this result, partial derivative of output stiffness with respect to joint angle is calculated to obtain joint input adjustment vector to achieve the commanded stiffness distribution (Fig. 2-(4)). The above process from (2) to (4) is cycled until the joint adjustment vector converged to enough small value. Due to this process for stiffness distribution control, output point of position control forced to deviate from commanded position. To compensate this error, learning control based on linear combination of error history [19] is employed.

In the following sections, detail of each process will be explained.

3. FORMULATION OF THE FLEXIBILITY CONTROL SCHEME

3.1. OUTPUT STIFFNESS ANALYSIS

As the first step of the flexibility control formulation, the output stiffness is obtained by iterative optimizing calculation. When input angles $\theta_{L1}, \ldots, \theta_{LN\ell}$ and $\theta_{R1}, \ldots, \theta_{RNr}$ are given to the actuator part, the position of each tip of the actuator part is obtained by direct kinematic analysis. Then the mechanical configuration of the spring part is obtained by minimizing potential energy stored in all torsion coil springs of spring constant k_i in the spring part. Since an initial mechanical configuration of the spring part which is geometrically appropriate to form a closed-loop can be obtained after the direct kinematic analysis of the actuator part, potential energy stored in the entire torsional springs is written as

$$E = \sum_{i=1}^{N_e} \frac{1}{2} k_i \theta_i^2 , \tag{2}$$

where θ_i is i-th joint angle of spring part. This potential energy, E, can be minimized based on gradient projection method [22]. When one of the ends of the spring part, J_1, is assumed as a virtual anchor joint, general solution of joint input of spring part and its partial derivative with respect to joint angle are written as

$$\dot{\boldsymbol{\theta}}_E = \boldsymbol{J}_{Ne}{}^{\#} \dot{\boldsymbol{r}}_{Ne} + \left(I - J_{Ne}{}^{\#} J_{Ne} \right) k \frac{\partial E}{\partial \theta} , \tag{3}$$

$$\frac{\partial E}{\partial \theta} = \begin{pmatrix} k_1 \theta_1 & \cdots & k_{Ne} \theta_{Ne} \end{pmatrix} , \tag{4}$$

where $\boldsymbol{\theta}_E = [\theta_1 \ \ \theta_2 \ \ldots \ \theta_{Ne}]^T$, J_{Ne} is a Jacobian matrix respect to N_e-th joint, the other tip of the spring part. $J_{Ne}{}^{\#} = J_{Ne}{}^T (J_{Ne} J_{Ne}{}^T)^{-1}$ is pseudo inverse of J_{Ne} . $\dot{\boldsymbol{r}}_{Ne}$ is a relative velocity against J_1. A joint input increment to minimize the potential energy, $\dot{\boldsymbol{\theta}}_E$, while holding both ends of the spring part at the tip of the actuator parts, is obtained by substituting $\dot{\boldsymbol{r}}_{Ne} = 0$ in equation (3).

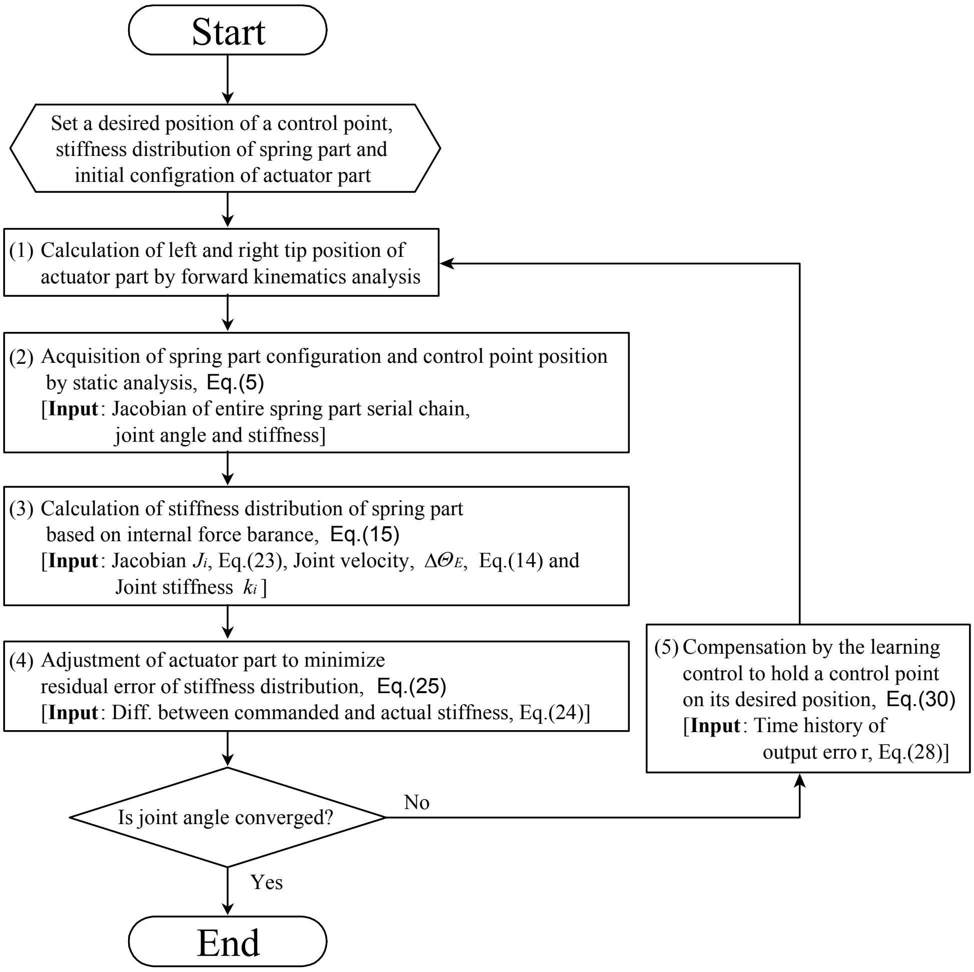

Fig. 2 – Process flow of the proposed simultaneous motion and stiffness distribution control.

$$\dot{\boldsymbol{\theta}}_E = k\left(I - J_{Ne}{}^{\#} J_{Ne}\right)\left(k_1\theta_1 \quad \cdots \quad k_{Ne}\theta_{Ne}\right)^{\mathrm{T}}, \tag{5}$$

where k is a negative constant. The mechanical configuration of the spring part is iteratively refreshed until $\dot{\boldsymbol{\theta}}_E$ become smaller than a threshold ε (=10.0×10^{-10} is the actual value used in the following simulations and experiments).

Fig. 4 illustrates an example of simulation result obtained from the above calculation scheme. In the simulation, design parameters of the mechanism are:

a) number of joints: $N_\ell = N_r = 2$ and $N_e = 6$,

b) link lengths of actuator part and spring part: 100 mm and 50 mm, respectively.

The actuator part moved from the configuration of (θ_{L1}, θ_{L2}, θ_{R1}, θ_{R2}) = (135, –90, 45, 90) degrees to (θ_{L1}, θ_{L2}, θ_{R1}, θ_{R2}) = (155, –75, 25, 75) degrees at constant angular velocity. In this case, the mechanism keeps symmetric configuration all the time, and exerted torque on each coil spring is equally distributed. By considering the relationship between the angular displacement of spring part and resulting torque written in equation (6),

$$\Delta\boldsymbol{\tau}_E = \mathrm{diag}(k_i)\Delta\boldsymbol{\theta}_E \,, \tag{6}$$

and by ignoring the effect of two tips of actuator part, all joint angles among spring part should be same when each i-th joint's spring constant, k_i, is common among entire spring part. The simulation result shown in Fig. 3 agrees with that prediction.

From the obtained spring part configuration, the output stiffness of each control point, K_i, can be calculated. Let us consider the i-th control point, P_i. The translation of the control point, ΔR_i, caused by an external force, F_i, can be described with respect to the output stiffness as

$$F_i = K_i \Delta R_i \,, \tag{7}$$

In this equation, F_i and ΔR_i are $M\times M$ matrices defined by M-base vectors as

$$F_i = \left(\boldsymbol{f}_{i,0} \cdots \boldsymbol{f}_{i,M}\right),\ \Delta R_i = \left(\Delta\boldsymbol{r}_{i,0} \cdots \Delta\boldsymbol{r}_{i,M}\right), \tag{8}$$

where $\boldsymbol{f}_{i,0}$ … $\boldsymbol{f}_{i,M}$ and $\Delta\boldsymbol{r}_{i,0}$ … $\Delta\boldsymbol{r}_{i,M}$ are independent each other, such like $\boldsymbol{f}_{i,0}$ and $\Delta\boldsymbol{r}_{i,0}$ are force and displacement on x axis, and $\boldsymbol{f}_{i,1}$ and $\Delta\boldsymbol{r}_{i,1}$ are that on y axis. Number of these independent vectors is same to degrees of freedom of workspace, M.

Since the torque increment of all joints to balance the external force is written as following Eq. (9), the external force F_i is derived from its deformation as Eq. (10).

$$\Delta T_E = J_i^{\mathrm{T}} F_i \,, \tag{9}$$

$$F_i = \left(J_i^{\mathrm{T}}\right)^{\#} \Delta T_E \,, \tag{10}$$

where J_i is a Jacobian matrix including closed-loop constraint. Procedure to obtain it will be explained later. Increment of torque, ΔT_E, and joint angle, $\Delta\Theta_E$, corresponding to the given displacement and force at control points are N_E by M matrices, defined by M-base vectors as

$$\Delta T_E = \left(\Delta\boldsymbol{\tau}_0 \cdots \Delta\boldsymbol{\tau}_M\right),\ \Delta\Theta_E = \left(\Delta\theta_0 \cdots \Delta\theta_M\right). \tag{11}$$

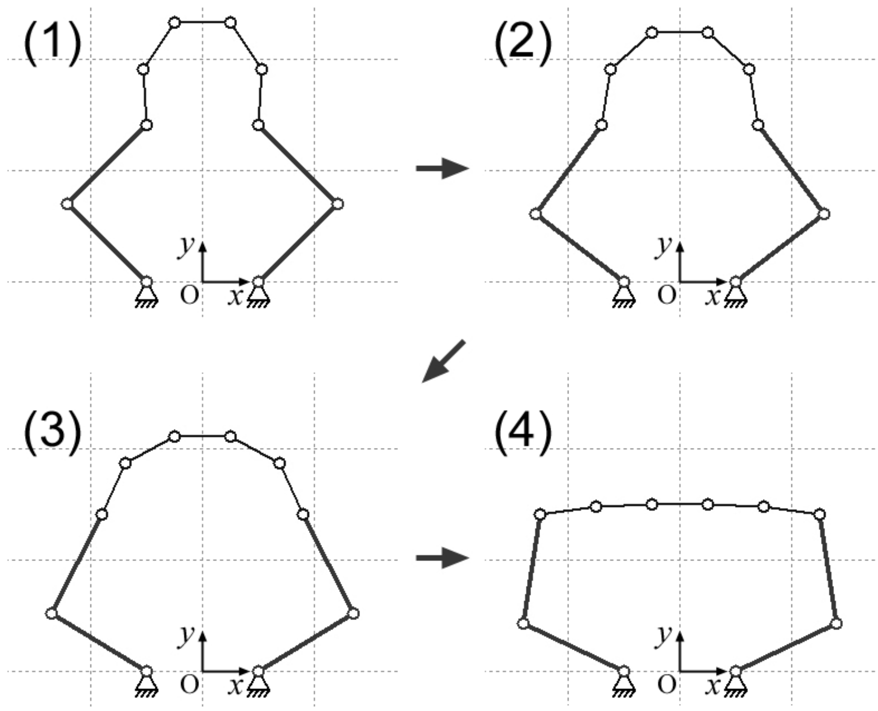

Fig. 3 – Simulation result obtained by the proposed forward kinematics analysis with minimizing of potential energy of the spring part.

Since the torque increment is also expressed by the spring constants and joint angles as

$$\Delta T_E = \mathrm{diag}(k_i)\Delta\Theta_E\,, \tag{12}$$

the external force F_i can be obtained by substituting equation (12) into eq. (10) as

$$F_i = \left(J_i^{\mathrm{T}}\right)^{\#}\mathrm{diag}(k_i)\Delta\Theta_E\,, \tag{13}$$

where

$$\Delta\Theta_E = \left(\Delta\boldsymbol{\theta}_0 \cdots \Delta\boldsymbol{\theta}_M\right). \tag{14}$$

By substituting equation (13) into eq. (7), the output stiffness K_i of the control point P_i can be derived as

$$K_i = \left(J_i^{\mathrm{T}}\right)^{\#}\mathrm{diag}(k_i)\Delta\Theta_E\Delta R_i^{-1} = \left(J_i^{\mathrm{T}}\right)^{\#}\mathrm{diag}(k_i)\Delta\Theta_E\left(J_i\Delta\Theta_E\right)^{-1}. \tag{15}$$

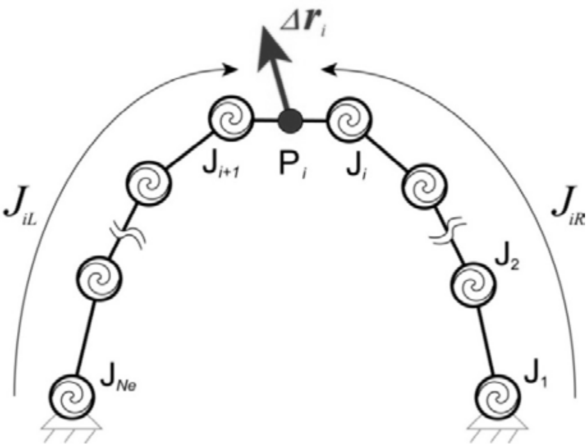

Fig. 4 – Closed-loop equation around a control point P_i .

To obtain a suitable Jacobian matrix J_i in equation (15), a velocity constraint condition should be applied in order to construct a closed-loop mechanism [23]. As illustrated in Fig. 4, the spring part can be split into left side part and right side part at the objective control point P_i . At this time, output velocity of the left part and the right part must agree. From this principle, the velocity constraint condition can be written as

$$\Delta \boldsymbol{r}_i = J_{iL} \Delta \boldsymbol{\theta}_L = J_{iR} \Delta \boldsymbol{\theta}_R \,, \tag{16}$$

where J_{iL} and J_{iR} are Jacobian matrices of the each serial kinematic chain on the left hand side and the right hand side respect to P_i, those assumes J_{Ne} and J_1 to temporal anchor joints. Equation (16) can be decomposed into column vectors $\boldsymbol{j}_{1,2,\ldots,i}$ and $\boldsymbol{j}_{i+1,i+1,\ldots,Ne}$ and scholar variables $\Delta\theta_{1,2,\ldots,i}$ and $\Delta\theta_{i+1,i+2,\ldots,Ne}$ then is organized into two groups, one is the elements those can be defined freely and the other should be constrained to establish a closed-loop. Since a planar translation is a 2DOF motion, two joint angles are constrained. Equation (16) can thus be rewritten as

$$\begin{aligned} J_{iL} &= \left[\boldsymbol{j}_{N_e} \quad \boldsymbol{j}_{N_e-1} \quad \cdots \quad \boldsymbol{j}_{i+1} \right], \\ J_{iR} &= \left[\mathbf{j}_1 \quad \mathbf{j}_2 \quad \cdots \quad \mathbf{j}_i \right], \\ \Delta \boldsymbol{\theta}_L &= \left[\Delta\theta_{N_e} \;\; \Delta\theta_{N_e-1} \; \cdots \; \Delta\theta_{i+1} \right]^{\mathrm{T}}, \\ \Delta \boldsymbol{\theta}_R &= \left[\Delta\theta_1 \;\; \Delta\theta_1 \; \cdots \; \Delta\theta_i \right]^{\mathrm{T}}, \end{aligned} \tag{17}$$

$$\begin{bmatrix} \boldsymbol{j}_{N_e} & \boldsymbol{j}_{N_e-1} \cdots \boldsymbol{j}_{i+2} & -\boldsymbol{j}_1 & -\boldsymbol{j}_2 \cdots -\boldsymbol{j}_{i-1} \end{bmatrix} \begin{bmatrix} \Delta\theta_{N_e} \\ \vdots \\ \Delta\theta_1 \\ \vdots \end{bmatrix} = \begin{bmatrix} -\boldsymbol{j}_{i+1} & \boldsymbol{j}_i \end{bmatrix} \begin{bmatrix} \Delta\theta_{i+1} \\ \Delta\theta_i \end{bmatrix}. \tag{18}$$

Equation (18) can be rewritten in a simple matrix form as

$$J_G \Delta\boldsymbol{\theta}_G = J_S \Delta\boldsymbol{\theta}_S , \tag{19}$$

where

$$\begin{aligned} J_G &= \begin{bmatrix} \boldsymbol{j}_{N_e} & \boldsymbol{j}_{EN_e-1} & \cdots \boldsymbol{j}_{i+2} & -\boldsymbol{j}_1 & -\boldsymbol{j}_2 & \cdots -\boldsymbol{j}_{i-1} \end{bmatrix}, \quad J_S = \begin{bmatrix} -\boldsymbol{j}_{i+1} & \boldsymbol{j}_i \end{bmatrix}, \\ \Delta\boldsymbol{\theta}_G &= \begin{bmatrix} \Delta\theta_{N_e} & \Delta\theta_{N_e-1} & \cdots & \Delta\theta_{i+2} & \Delta\theta_1 & \Delta\theta_2 \cdots \Delta\theta_{i-1} \end{bmatrix}^{\mathrm{T}}, \quad \Delta\boldsymbol{\theta}_S = \begin{bmatrix} \Delta\theta_{i+1} & \Delta\theta_i \end{bmatrix}^{\mathrm{T}}. \end{aligned} \tag{20}$$

The joint angle increment $\Delta\boldsymbol{\theta}_S$ which satisfies the velocity constraint condition is obtained by transforming equation (19) as

$$\Delta\boldsymbol{\theta}_S = J_S{}^{\#} J_G \Delta\boldsymbol{\theta}_G = H \Delta\boldsymbol{\theta}_G = \begin{bmatrix} \boldsymbol{h}_1 \\ \boldsymbol{h}_2 \end{bmatrix} \Delta\boldsymbol{\theta}_G , \tag{21}$$

where H is a Jacobian matrix which describes the influence of the arbitrary defined element $\Delta\boldsymbol{\theta}_G$ against the constrained elements $\Delta\boldsymbol{\theta}_S$. The composing vectors $\boldsymbol{h}_1$ and $\boldsymbol{h}_2$ are row vectors, size of $(N_e - 2)$. From equation (21), each element of $\Delta\boldsymbol{\theta}_s$ that satisfies the closed-loop constraint is obtained as

$$\Delta\theta_{i+1} = \boldsymbol{h}_1 \Delta\boldsymbol{\theta}_G, \quad \Delta\theta_i = \boldsymbol{h}_2 \Delta\boldsymbol{\theta}_G . \tag{22}$$

From above, the Jacobian matrix, J_i , which satisfies the velocity constraint condition is obtained as

$$\begin{bmatrix} -J_S & J_G \end{bmatrix} \begin{bmatrix} \Delta\boldsymbol{\theta}_S \\ \Delta\boldsymbol{\theta}_G \end{bmatrix} = \begin{bmatrix} H & J_G \end{bmatrix} \Delta\boldsymbol{\theta}_G, \quad J_i = \begin{bmatrix} H & J_{\mathrm{G}} \end{bmatrix}. \tag{23}$$

3.2. SIMULTANEOUS ACHIEVEMENT OF OUTPUT POSITION AND STIFFNESS DISTRIBUTION

A stiffness distribution control is carried out by minimizing the accumulated residual error in-between the desired output stiffness ${}^{d}K_i$ and actual output stiffness K_i, obtained in equation (15). The objective function to be minimized is

$$\phi(\boldsymbol{\theta}_E) = \mathrm{trace}\left({}^dK_i - K_i\right). \tag{24}$$

Angular input for each joint of the spring part to minimize the objective function is obtained from the partial derivative of equation (24) with respect to joint angle as

$$\dot{\theta}_i = k\frac{\partial\phi}{\partial\theta} = k\,({}^dK_i - K_i)\frac{\partial K_i}{\partial\theta}, \tag{25}$$

where

$$\frac{\partial K_i}{\partial\theta} = \left(\frac{\partial J_i}{\partial\theta}\right)\left(k_1\theta_1\cdots k_{Ne}\theta_{Ne}\right)^{\mathrm{T}} + J_i\left(k_1\cdots K_{Ne}\right)^{\mathrm{T}}, \tag{26}$$

k (= –0.01 in below) is a negative constant. An angular joint input velocity of the spring part can thus be obtained as

$$\dot{\boldsymbol{\theta}}_E = \begin{bmatrix}\cdots & \dot{\theta}_i & \cdots\end{bmatrix}^{\mathrm{T}}. \tag{27}$$

Since the spring part is a passive mechanism, the obtained joint input cannot be given to the robot directly. Thus the obtained input needs to be converted to tip translation of each actuator part, $\Delta\boldsymbol{r}_1$ and $\Delta\boldsymbol{r}_{Ne}$ as shown in Fig. 5, to achieve the desired stiffness distribution. Although an output point of position control that is chosen among a number of control points should be held at a desired position, the stiffness distribution control tends to push the output point out from a desired position. An additional input is thus necessary to keep the output point in position. The learning control scheme based on linear combination of error history [12] is used to achieve this compensation. During the iterative calculation of spring part configuration, the output error of the main task, $\Delta\boldsymbol{e}_{n,j}$, shown as dashed allow in Fig. 5, is calculated as

$$\begin{aligned}
\boldsymbol{e}_{n-1,j} &= {}^d\boldsymbol{r}_{j-1} - \boldsymbol{r}_{n-1,j}, \\
\boldsymbol{e}_{n-1,j-1} &= {}^d\boldsymbol{r}_{j-1} - \boldsymbol{r}_{n-1,j-1}, \\
\boldsymbol{e}_{n,j-1} &= {}^d\boldsymbol{r}_{j} - \boldsymbol{r}_{n-1,j},
\end{aligned} \tag{28}$$

where n and j are an iteration count number and a reference point number which refers the current position of the output point on a desired trajectory, respectively.

As illustrated in Fig. 6, the obtained errors are stored as output error history so as to calculate the displacement compensation input as

$$\Delta^d\boldsymbol{r}_{n,j} = \Delta\boldsymbol{r}_{n-1,j} + C_0\boldsymbol{e}_{n,j-1} - C_1\boldsymbol{e}_{n-1,j-1} + C_2\boldsymbol{e}_{n-1,j}, \tag{29}$$

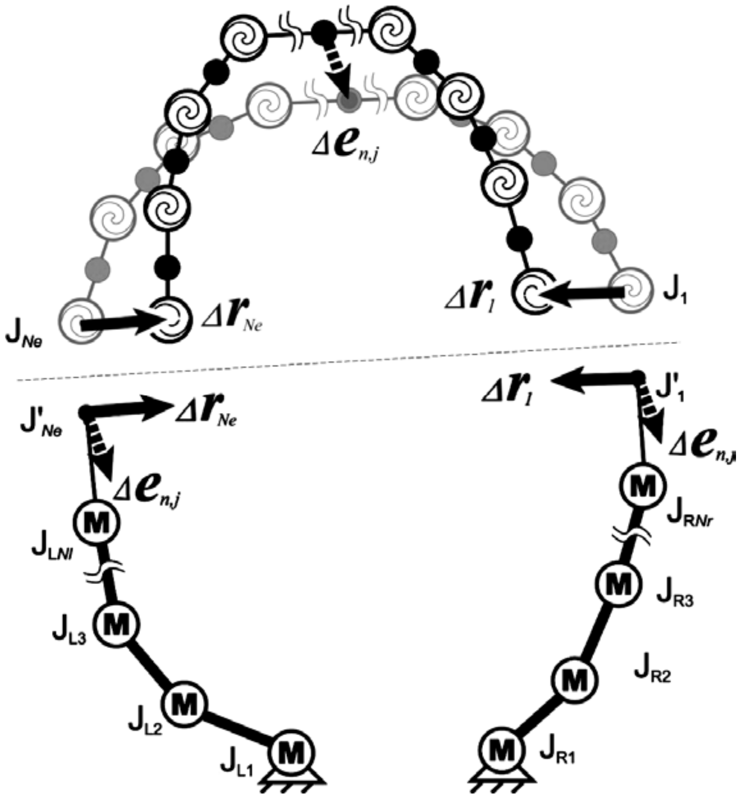

Fig. 5 – Disturbance of output position due to the stiffness distribution control and corresponding output error.

where C_0, C_1 and C_2 are learning coefficients ranging $0<C_0,\ C_2<1$ and $-1<C_1<0$. The actuator joint angle input to achieve this displacement can be obtained as

$$\begin{aligned}\Delta\boldsymbol{\theta}_{Ln,j} &= \Delta\boldsymbol{\theta}_{Ln-1,j} + J_L{}^{\#}\left(C_0\boldsymbol{e}_{n-1,j} + C_1\boldsymbol{e}_{n-1,j-1} + C_2\boldsymbol{e}_{n,j-1}\right),\\ \Delta\boldsymbol{\theta}_{Rn,j} &= \Delta\boldsymbol{\theta}_{Rn-1,j} + J_R{}^{\#}\left(C_0\boldsymbol{e}_{n-1,j} + C_1\boldsymbol{e}_{n-1,j-1} + C_2\boldsymbol{e}_{n,j-1}\right).\end{aligned} \tag{30}$$

The flexibility control is carried out by the simultaneous execution of the stiffness distribution control scheme and the learning control scheme.

4. FLEXIBILITY CONTROL EXPERIMENT

4.1. STIFFNESS DISTRIBUTION CONTROL

The proposed flexibility control scheme was validated by experiments with a 10R elastic closed-loop robot shown in Fig. 7. The actuator part of this robot is composed of 100mm long links and four actuator units; 5W-output DC motors, optical encoders that generate 512 pulses per revolution and harmonic reducers

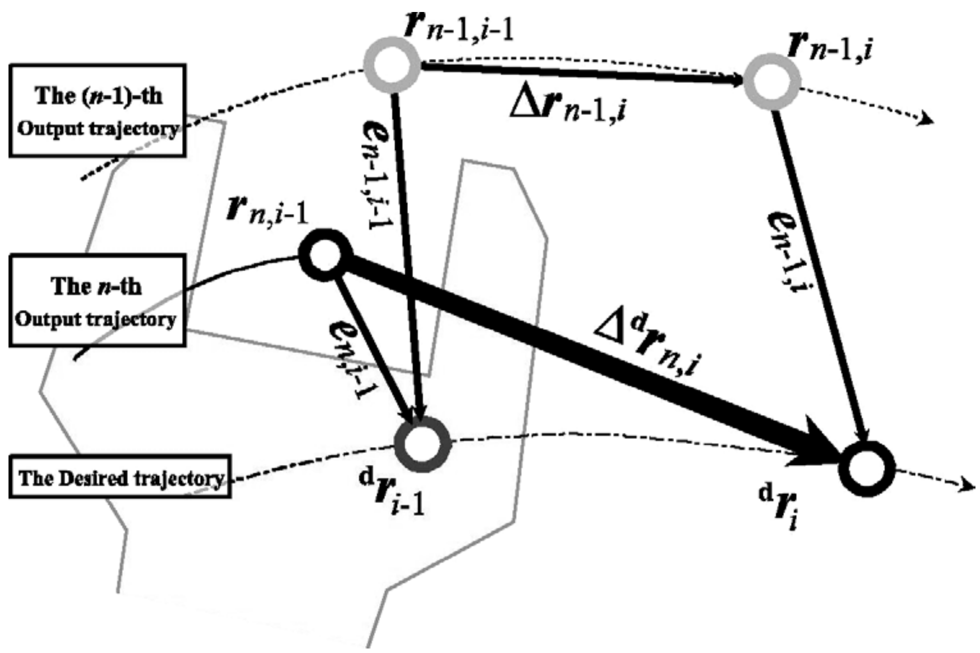

Fig. 6 – Target trajectory, output trajectory at two trials, error vectors and compensation vector of the learning control scheme based on linear combination of error history.

with a reduction ratio of 100:1. The spring part is a serial chain of six revolute joints connected by 50 mm long links. Each of them has a torsion coil spring with a stiffness of 2.0 N·mm/deg. Three control points, P_1, P_2 and P_3 are set on the each center of three links of the spring part. Target stiffness distributions were given to these three control points so as to deal with various contact conditions appropriately.

In the first experiment, converged solution was calculated was evaluated by comparing the commanded stiffness distributions and actual output stiffness at each control point. In this experiment, direction of external load for each control point was assumed to be orthogonal against the static link, namely parallel to the y axis, and three target stiffness distributions; (i) ${}^dK_1 = {}^dK_3 =(0,1000)$ N/m, ${}^dK_2 =(0,500)$ N/m, (ii) ${}^dK_1={}^dK_2={}^dK_3=(0,300)$ N/m and (iii) ${}^dK_1={}^dK_3=(0,10)$ N/m, ${}^dK_2=(0,1000)$ N/m were given. In this experiment, only the stiffness on y axis was evaluated but command value on x axis was also given to obtain a solution by the proposed scheme. Actual output stiffness on y axis was measured by the setup shown in Fig. 8.

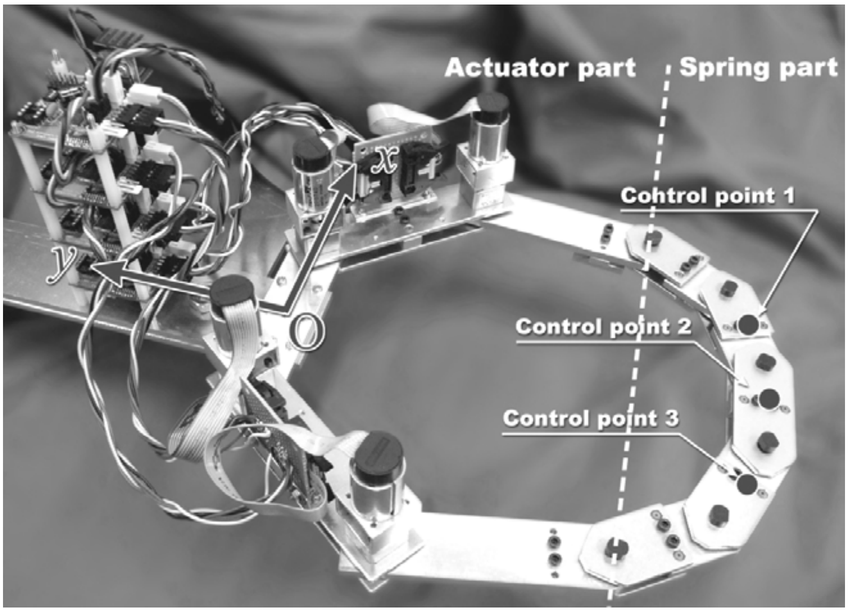

Fig. 7 – Prototype 10R elastic closed-loop robot.

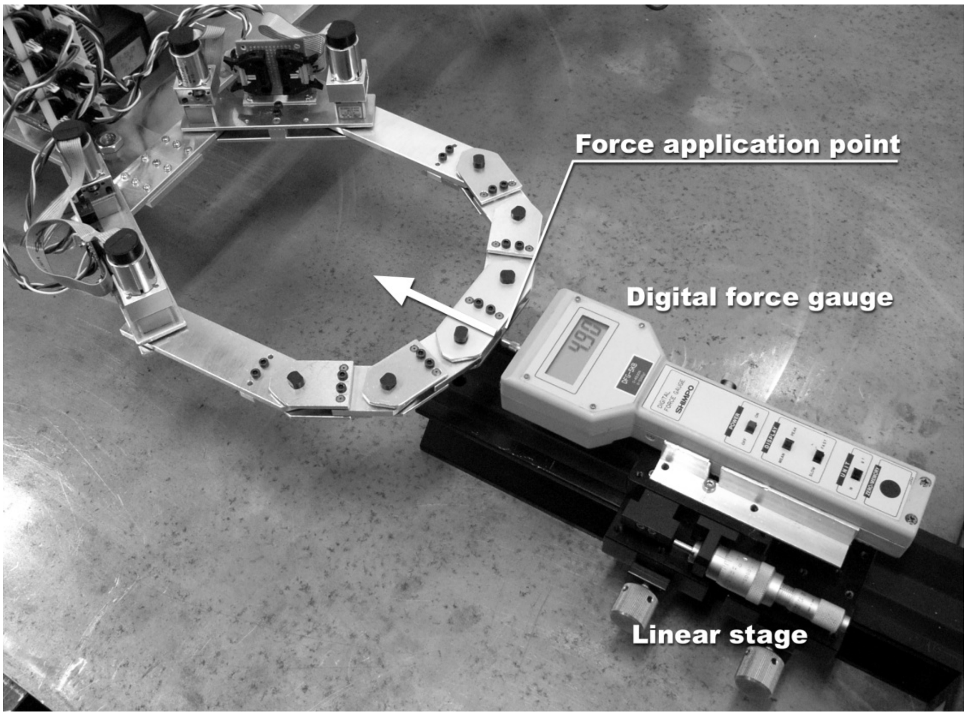

Fig. 8 – Setup of the stiffness distribution measurement experiment.

Probe of a force gauge fixed on a linear stage so that it can press each control point to measure the relationship between the given displacement and reaction force. The obtained output stiffness shown in Fig. 9 almost agrees to the each target values, except ${}^{d}K_1$ and ${}^{d}K_3$ in the setting (iii). In this case, since the output stiffness K_2 was large due to the commanded value, and consequently K_1 and K_3 also become large, almost infinite in the preliminary simulation. This means that some target stiffness settings cannot be achieved when they are extremely large or small. However, the effectiveness of the proposed stiffness control scheme has been confirmed and the elastic closed-loop robot could achieve various stiffness distributions.

4.2. OBJECT GRASPING EXPERIMENT

In the second experiment, a pair of robots grasped target objects in-between their spring parts to demonstrate the effectiveness of the flexibility control scheme for the achievement of adaptive contact. The target objects were a sponge cube and an octagonal Styrofoam beam, and the above stiffness distributions (i) and (iii) were applied. In this experiment, the center control point P_2 was chosen as an output point of the position control. A desired trajectory, which makes two spring parts closer, was given to grasp the target objects. The stiffness distribution (i) can achieve highly adaptive contact against arbitrary shaped objects because the center contact area stiffness is lower than outside; the distribution (iii) can achieve strong grasping because the output stiffness of entire contact area is high, thus the mechanism becomes rigid against the external force. It should be noted that after contacting to an object, shape of the spring part will change and stiffness distribution will also be change. In order to achieve precise control of the output stiffness distribution, this effect should be considered. However, it can be ignored just to establish different kind of grasping with open-loop control as long as stiffness of spring part is extremely high or low, just like the selected configuration in this experiment.

Snapshots of the obtained trajectory at the beginning and the end of each grasping motion are shown in Fig. 10. The translation and rotation of the target objects after the robot began to contact were measured by image analysis using the vertexes of the polygonal target shape. The obtained translation and rotation are shown in Fig. 10. Since the flexibility of the entire system, which includes the target object and the robot itself, dominates the amplitude of the translation of the object, the sponge cube moved larger than the Styrofoam beam, and it also can be seen that the stiffness distribution (iii) makes the translation distance smaller.

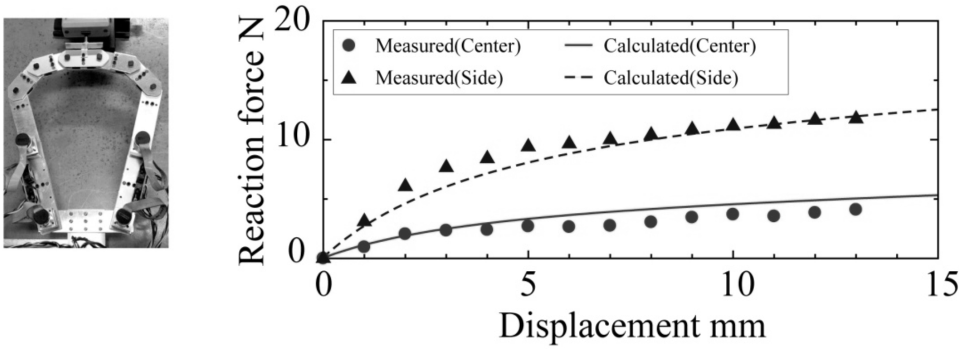

(i) ${}^{d}K_1$, ${}^{d}K_3$=(0,1000) N/m, ${}^{d}K_2$=(0,500) N/m

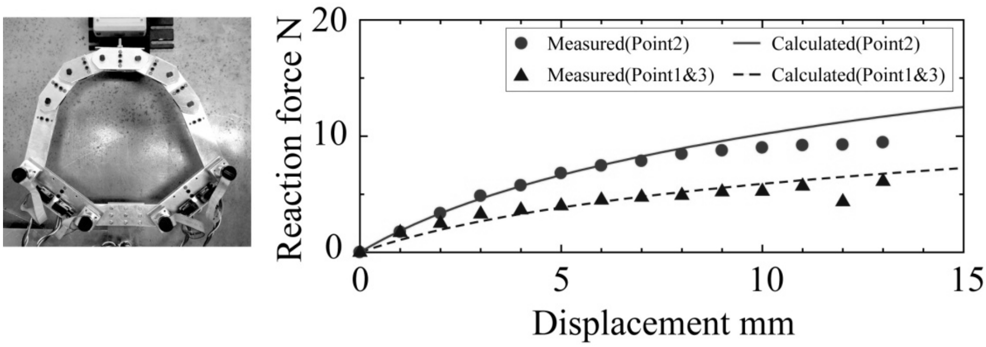

(ii) ${}^{d}K_1$, ${}^{d}K_2$, ${}^{d}K_3$=(0,300) N/m

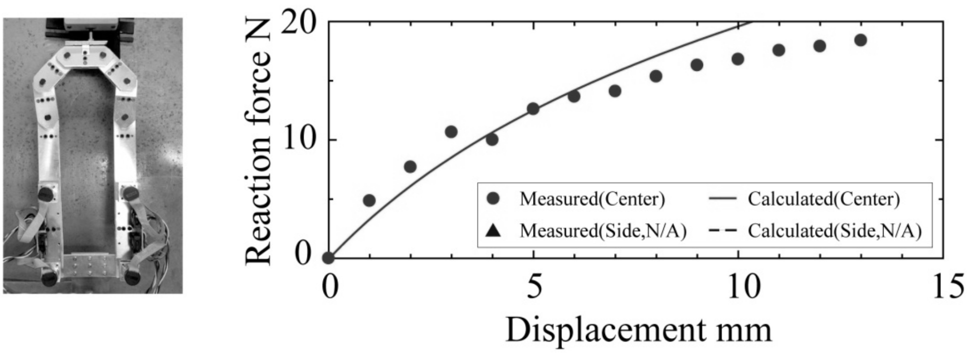

(iii) ${}^{d}K_1$, ${}^{d}K_3$=(0,10) N/m, ${}^{d}K_2$=(0,1000) N/m

Fig. 9 – Obtained mechanical configurations (left) and output stiffness distributions (right) under the three target stiffness distribution combinations.

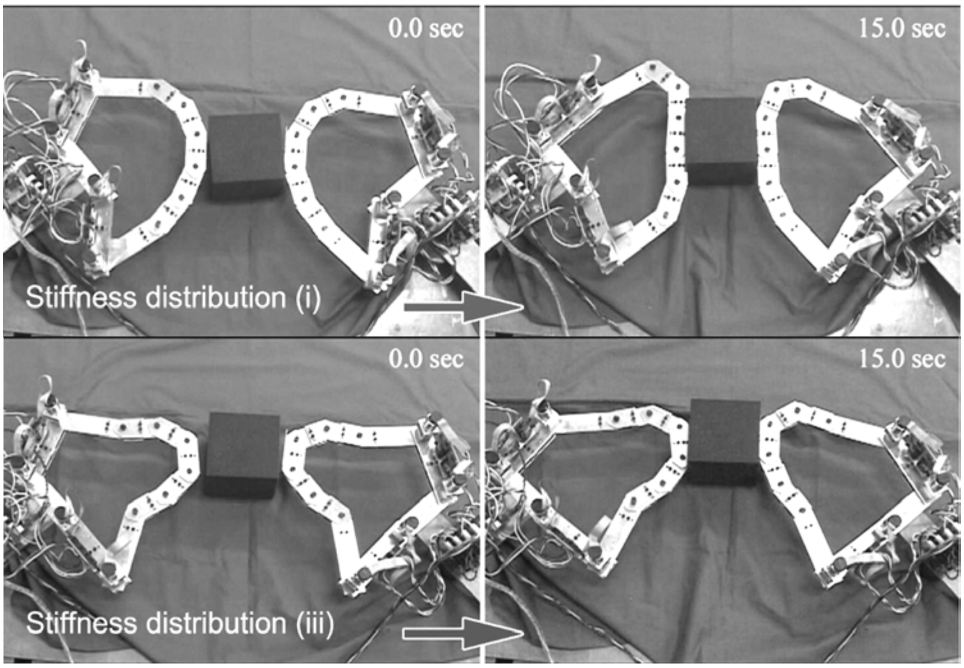

a) grasping of a sponge cube

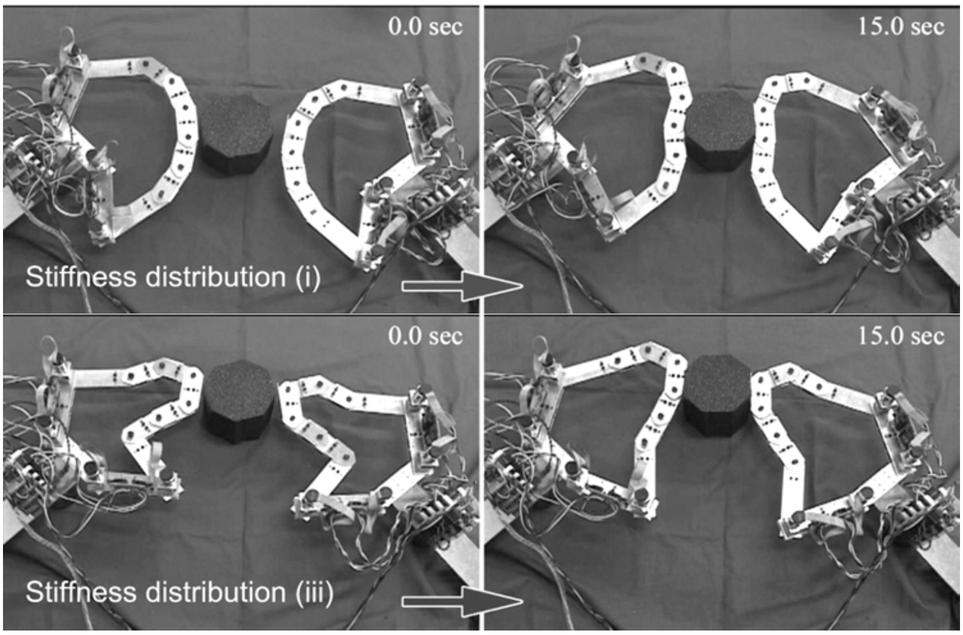

b) grasping of an octagonal Styrofoam beam

Fig. 10 – Snapshots of the output trajectory in the object grasping experiment.

Therefore, it can be said that a strong grasping with high stiffness distribution is effective to achieve stable grasping of soft objects. On the other hand, when the robot tried to grasp the Styrofoam beam, reaction of the object became unstable, since unpredictable slip was frequently occurred. This slip appears as a rapid change of the rotation angle in Fig. 11, and the fluctuation was smaller when the distribution (i) was applied than in case of distribution (iii). Therefore it can be said that a soft grasping with low stiffness distribution is effective to achieve stable grasping of hard and slippy object because contact force spread out among wide area equally so as to enable a robot to follow arbitrary object shapes.

5. CONCLUSIONS

In this paper, a motion control scheme called flexibility control, which aims to achieve motion control of specific control point and force application at multiple contact points simultaneously, is proposed. An elastic redundant closed-loop manipulator was designed to achieve this concept, and control scheme was established. Obtained results are summarized as followings.

(1) A lightweight and supple elastic redundant closed-loop robot having two serial chains of active joints called “actuator part” and one serial chain of passive joints with torsion coil springs called “spring part” was designed to as an effective solution to achieve a large workspace and to realize the flexibility control concept.

(2) Process flow of the flexibility control was figured out. The scheme includes [i] Direct analysis of the actuator part and spring part, [ii] Stiffness analysis of the spring part, [iii] Adjustment of joint angle to achieve commanded stiffness distribution of spring part, and [iv] Learning control based on linear combination of error history to achieve commanded position of a specific control point within the spring part.

(3) Direct analysis of the mechanism is performed by combining the kinemics analysis of the actuator part and minimization of the summation of potential energy stored in torsional springs. Output stiffness at each control point is acquired by considering the balance of internal force among the springs and velocity constraints to form a closed-loop.

(4) Simultaneous control of stiffness distribution among a number of control points and output position of a specific point among them was formulated by joint angle adjustment input based on the partial derivative of the output stiffness with respect to joint angle, and the learning control scheme based on linear combination of error history.

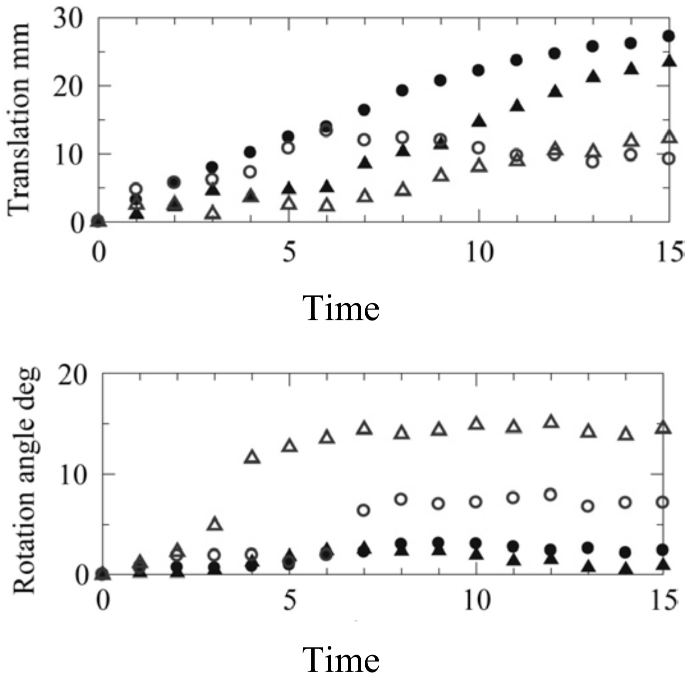

Fig. 11 – Relative translation (top) and rotation (bottom) of the target object.

(5) By using a prototype 10R elastic redundant closed-loop manipulator, output stiffness distribution control experiments and object grasping experiments were performed to demonstrate the effectiveness of the proposed control scheme. The prototype robot achieved commanded output stiffness distribution and various contact motions that could adapt to different contact conditions.

Received on December 15, 2012

REFERENCES

1. KHATIB, O., *A Unified Approach for Motion and Force Control of Robot Manipulators: The Operational Space Formulation*, IEEE Journal of Robotics and Automation, **RA-3**, *1*, pp. 43-53, 1987.
2. XIAO, D., GHOSH, B.K., XI, N., TARN, T.J., *Sensor-Based Hybrid Position/Force Control of a Robot Manipulator in an Uncalibrated Environment*, IEEE Transactions on Control Systems Technology, **8**, *4*, pp. 635-645, 2000.
3. KOCK, S., SCHUMACHER, W., *Control of a Fast Parallel Robot with a Redundant Chain and Gearboxes: Experimental Results*, IEEE Proc. of the 2000 IEEE International Conference on Robotics and Automation, pp. 1924-1929, 2000.
4. NEMEC, B., ZLAJPAH, L., *Force Control of Redundant Robots in Unstructured Environment*, IEEE Transactions on Industrial Electronics, **49**, *1*, pp. 233-240, 2002.

5. WU, C.H., *Compliance Control of a Robot Manipulator Based on Joint Torque Servo*, The International Journal of Robotics Research, **4**, *3*, pp. 55-71, 1985.
6. YOKOI, K., MAEKAWA, H., TANIE, K., *A Method of Compliance Control for a Redundant Manipulator*, Proc. of IEEE/RSJ International Conference on Intelligent Robots and Systems, **3**, pp. 1927-1934, 1992.
7. ZOLLO, L., SICILIANO, B., DE LUCA, A., GUGLIELMELLI, E., DARIO, P., *Compliance Control for an Anthropomorphic Robot with Elastic Joints: Theory and Experiments*, ASME Journal of Dynamic Systems, Measurement, and Control, **127**, pp. 321-328, 2005.
8. HOGAN, N., *Impedance Control: An Approach to Manipulation: Part 1.3*, Transactions of the ASME, Journal of Dynamic Systems, Measurement and Control, **107**, pp. 1-24, 1985.
9. MUSSA-IVALDI, F.A., *Integrable Solutions of Kinematic Redundancy via Impedance Control*, The International Journal of Robotics Research, **10**, *5*, pp. 481-491, 1991.
10. ALBU-SCHAFFER, A., OTT, C., FRESE, U., HIRZINGER, G., *Cartesian Impedance Control of Redundant Robots: Recent Results with the DLR-light-weight-arms*, Proc. of IEEE International Conference on Robotics and Automation (ICRA03), **3**, pp. 3704-3709, 2003.
11. ALI, S., MOOSAVIAN, A., MOSTAFAVI, M., *Multiple Impedance Control of Redundant Manipulators*, Proc. of IEEE Conference on Robotics, Automation and Mechatronics, pp. 1-6, 2006.
12. LAURIN-KOVITZ, K.F., COLGATE, J.E., CARNES, S.D.R., *Design of Components for Programmable Passive Impedance*, Proc. of IEEE International Conference on Robotics and Automation, pp. 1476-1481, 1991.
13. MORITA, T., SUGANO, S., *Development of 4-DOF manipulator using mechanical impedance adjuster*, Proc. of 1996 IEEE International Conference on Robotics and Automation, **4**, pp. 2902-2907, 1996.
14. HIROAKI, K., HYODO, K., OGANE, D., *On Tendon-Driven Robotic Mechanisms with Redundant Tendons*, The International Journal of Robotics Research, **17**, *5*, pp. 561-571, 1998.
15. TATARA, Y., *On Compression of Rubber Elastic Sphere over a Large Range of Displacements-Part I: Theoretical Study*, Transactions of the ASME, Journal of Engineering Materials and Technology, **113**, pp. 285-291, 1991.
16. XYDAS, N., KAO, I., *Modeling of Contact Mechanics and Friction Limit Surfaces for Soft Fingers in Robotics, with Experimental Results*, International Journal of Robotics Research, **18**, *8*, pp. 941-950, 1999.
17. NAGASE, K., NAKASHIMA, A., HAYAKAWA, Y., SOBAJIMA, K., *Control of Grasping and Manipulation of an Object with Soft Finger-tips*, Transactions of the Society of Instrument and Control Engineers, **40**, *5*, pp. 518-527, 2004.
18. INOUE, T., HIRAI, S., *Elastic Model of Deformable Fingertip for Soft-Fingered Manipulation*, IEEE Transactions on Robotics, **22**, *6*, pp. 1273-1279, 2006.
19. MATSUURA, D., IWATSUKI, N., *Motion Control of Hyper Redundant Robots by Learning Control Based on Linear Combination of Error History and Initial Configuration Optimization with Backward Learning*, Journal of Advanced Mechanical Design, Systems, and Manufacturing, **2**, *6*, pp. 1011-1020, 2008.
20. MATSUURA, D., IWATSUKI, N., OKADA, M., *Redundancy Optimization of Hyper Redundant Robots Based on Movability and Assistability*, Journal of Advanced Mechanical Design, Systems, and Manufacturing, **2**, *6*, pp. 1021-1029, 2008.
21. MATSUURA, D., IWATSUKI, N., OKADA, M., *Development of an Elastic Redundant Closed-Loop Robot Manipulator and Its Flexibility Control*, CD-ROM Proc. of IEEE/RSJ 2009 International Conference on *Intelligent Robots and Systems* (IROS 2009), 2009, pp. 351-356.
22. DUBEY, R.V., EULER, J.A., BABCOCK, S.M., *An Efficient Gradient Projection Optimization Scheme for a Seven-degree-of-freedom Redundant Robot with Spherical Wrist*, Proc. of IEEE Int. Conf. on *Robotics and Automation*, 1988, pp. 28-36.
23. YAMANE, K., NAKAMURA, Y., *Dynamics Computation of Structure-Varying Kinematic Chains for Motion Synthesis of Humanoid*, Proc. of IEEE International Conference on *Robotics and Automation*, 1999, pp. 714-721.